Modeling the Electrical and Thermal Response of Superconducting Nanowire Single-Photon Detectors

Joel K. W. Yang, Andrew J. Kerman, Eric A. Dauler, Vikas Anant, Kristine M. Rosfjord, and Karl K. Berggren

***Abstract*—We modeled the response of superconducting nanowire single-photon detectors during a photodetection event, taking into consideration only the thermal and electrical properties of a superconducting NbN nanowire on a sapphire substrate. Our calculations suggest that heating which occurs after the formation of a photo-induced resistive barrier is responsible for the generation of a measurable voltage pulse. We compared this numerical result with experimental data of a voltage pulse from a slow device, i.e. large kinetic inductance, and obtained a good fit. Using this electro-thermal model, we estimated the temperature rise and the resistance buildup in the nanowire, and the return current at which the nanowire becomes superconducting again. We also show that the reset time of these photodetectors can be decreased by the addition of a series resistance and provide supporting experimental data. Finally we present preliminary results on a detector latching behavior that can also be explained using the electro-thermal model.**

***Index Terms*—Electro-thermal model, nanowire, niobium nitride, single-photon detector.**

I. Introduction

SUPERCONDUCTING nanowire single-photon detectors (SNSPD) have recently demonstrated 57% detection efficiency [1], jitter of ~30 ps [2] and dark counts of ~100 counts/s [3]. These devices operate based on the local suppression of superconductivity along a nanowire after the absorption of a photon [4]. By biasing the nanowire with a current $I_{\rm bias}$ close to (but less than) its critical current $I_{\rm c}$, the photo-induced suppression in superconductivity leads to the formation of a resistive barrier along the nanowire and results in a measurable voltage pulse across the SNSPD.

The detailed physics of the detection process is still unclear. Presently, theories on superconducting detectors do not explain the substantial resistance built-up in a nanowire that happens after photon absorption. In this paper, we propose a simple electro-thermal mechanism to explain the processes that occur after a narrow resistive barrier forms along the nanowire. In this model, Joule heating due to current flowing through this resistive barrier provides the energy for the growth of a normal segment along the wire.

We approximated the SNSPD as a one-dimensional structure and modeled the thermal response using a one-dimensional time-dependent heat equation. The electrical behavior was modeled by treating the SNSPD as an inductor (from its kinetic inductance) in series with a current and temperature-dependent resistor. Using this relatively simple model, we showed that the electro-thermal dynamics result in a measurable voltage pulse.

We recently showed in [5] that the reset time of SNSPDs is limited by its kinetic inductance $L_{\rm k}$. This limitation implies that any effort to increase the SNSPD detection efficiency, i.e. by increasing the meander fill factor for wires of a constant width [6] or fabricating narrower wires with the same fill factor would result in a slower device. In this paper, we present preliminary experimental results on a method that breaks this speed limitation. We demonstrate a speed-up in SNSPD response by a factor of five resulting from the addition of a resistor in series with the device.

Finally, we discuss a device latching behavior that could present a new speed limitation to the SNSPDs. We experimentally observed that latching will occur when one uses a large enough series resistor with the device. We show that our electro-thermal model produces a qualitatively similar trend.

II. Thermal and Electrical Model

A. Thermal Model

Presently, models of superconducting devices consider either the microscopic non-equilibrium relaxation mechanism in a superconductor [7], [8] or the static thermal properties of a superconducting nanowire [9], [10]. However, these approaches have neglected the dynamic interaction between the electrical and thermal systems. For instance, they do not account for the growth and collapse of a normal segment in the wire, an effect which we know must occur in order to produce a measurable voltage pulse across our detectors.

We propose a thermal model that is simple because we consider only the macroscopic thermal properties of the NbN nanowire and the sapphire substrate. This thermal model is a time-dependent extension of the steady-state heat equation used in studying self-heating in superconducting wires (see for example, [10]).

We modeled the heat flow resulting from Joule heating when a large bias current ($\sim 16\ \mu$A) flows through a photo-induced resistive barrier in the nanowire. The heat flow that we considered in the thermal model is as shown in Fig. 1(a). Heat generated by Joule heating flows along the wire and into the

Manuscript received August 28, 2006. This work was supported by the U.S. Air Force under Air Force Contract FA8721-05-C-002.

Opinions, interpretations, recommendations, and conclusions are those of the authors and are not necessarily endorsed by the United States Government.

J. K. W. Yang, E. A. Dauler, V. Anant, K. M. Rosfjord, and K. K. Berggren are with the Massachusetts Institute of Technology, Cambridge, MA 02139 USA (e-mail: ykwjoel@mit.edu).

A. J. Kerman is with the Lincoln Laboratory, Massachusetts Institute of Technology Lexington, MA 02420 USA.

Color versions of one or more of the figures in this paper are available online at http://ieeexplore.ieee.org.

Digital Object Identifier 10.1109/TASC.2007.898660

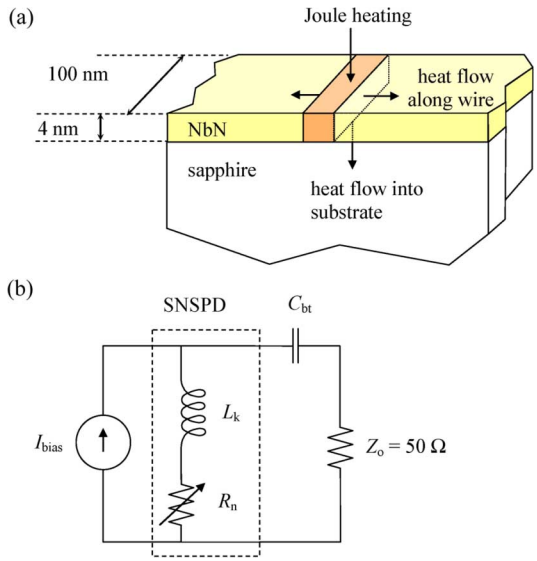

Fig. 1. (a) Schematic of the thermal model used in our simulation. Using a finite difference method, we treated the nanowire as a quasi-one-dimensional structure with many discrete Δx segments and solved a 1-D time-dependent heat equation for the entire wire. The temperature at each segment and the current flowing through the wire were used to determine if the segment under consideration switches into the normal/resistive state or remains superconducting. (b) A simplified electrical of the SNSPD connected in a typical testing configuration. The SNSPD was modeled as an inductor in series with a resistor, whose value depends on the current through the device and the local wire temperature as determined from the thermal model. The capacitor models the AC branch of a bias tee used in our setup and the transmission line that carries the signal to measurement instruments was modeled as a 50 Ω impedance.

substrate while simultaneously increasing the local temperature of the heated region. The structure used in our model was a 4-nm-thick and 100-nm-wide NbN wire on a sapphire substrate. Using a finite difference numerical method, the length of nanowire was divided into discrete segments of length Δx. We studied a simple case where a 15-nm-long segment of wire initially becomes normal (roughly the thermalization length of the hotspot [4], [11]), and calculated the subsequent temperature change for every segment of the wire. As the current density is uniform along the width of the wire, Joule heating should also occur uniformly and hence we only considered a single temperature for each Δx segment. The temperature T of each segment was solved using the time-dependent one-dimensional heat equation,

$$J^2\rho + \kappa\frac{\partial^2 T}{\partial x^2} - \frac{\alpha}{d}(T - T_{\rm sub}) = \frac{\partial cT}{\partial t}, \tag{1}$$

where J is the current density through the wire; ρ is the electrical resistivity, which is non-zero where the wire is normal and zero where the wire is superconducting; κ is the thermal conductivity of NbN; α is the thermal boundary conductivity between NbN and sapphire; d is the wire thickness; $T_{\rm sub}$ is the substrate temperature and c is the specific heat per unit volume of NbN. The first term on the left hand side of (1) is the heat generated due to Joule heating; the second term is the heat dissipated by thermal conduction along the wire; the third term is the heat dissipated into the substrate; and the term on the right hand side of (1) is the rate of change in the local energy density. From (1), we see that the relative proportion of energy transferred along the wire, into the substrate or as a local temperature increase depends on the magnitudes of α, κ and c respectively.

The difficulty in solving (1) stems from the dependence of ρ, κ, α and c on temperature and on the normal or superconducting state of the wire. For instance, ρ of a region along the wire at temperature T is zero when the current through that region is less than the critical current at that temperature $I_{\rm c}(T)$. In our simulations, we used a phenomenological expression to calculate $I_{\rm c}$(T),

$$I_{\rm c}(T) = I_{\rm c}(0)\left(1 - \left(\frac{T}{T_{\rm c}}\right)^2\right)^2, \tag{2}$$

where the critical temperature, $T_{\rm c} = 10.5$ K for our 4-nm-thick NbN film and $I_{\rm c}(0) = 20\ \mu$A for a 100-nm-wide wire. The bias current was set to 90% of $I_{\rm c}(T_{\rm sub})$. Equation (2) was obtained from an excellent fit with experimental measurements over the range of temperatures from 2 K to $T_{\rm c}$. We assumed that this expression, generally true in steady state, can also be extended to the nanosecond time scales that we consider. Using this expression, we define a segment as being resistive when $I > I_{\rm c}(T)$ and assign a constant nonzero value of $\rho = R_\gamma d$ to that segment; where $R_\gamma = 600\ \Omega/\gamma$ is the measured sheet resistance of the 4-nm-thick NbN film. We do this check and assignment in our simulation for each wire segment and at each time step.

We included both the electron and phonon specific heat of NbN in our model. The electron specific heat of NbN $c_{\rm e}$ was taken to be state and temperature dependent. The expression we used to calculate the normal state electron specific heat $c_{\rm en}$ of a resistive wire segment is as follows:

$$c_{\rm en} = \gamma T \tag{3}$$

On the other hand, the superconducting electron specific heat $c_{\rm es}$ was calculated using the following expression:

$$c_{\rm es} = Ae^{-\frac{\Delta}{kT}} \tag{4}$$

where A is a proportionality constant that is calculated such that $c_{\rm s}(T_{\rm c}) = 2.43c_{\rm n}(T_{\rm c})$ [12]. The phonon specific heat $c_{\rm p}$ was taken to be state independent and proportional to T^3. The specific heat values we used in our model were obtained from [11].

The thermal boundary conductivity α between NbN and sapphire determines the rate at which heat is conducted away into the substrate. In a microscopic sense α determines the phonon escape time from the film. We ignored the state dependence of α and only considered its cubic dependence on temperature (see [13] for example), i.e. $\alpha = BT^3$. However, measurements of thermal boundary resistance (i.e. $1/\alpha$) of Al on sapphire [14] have shown that α was strongly state dependent. We argue that this dependence is not important in our model, as most of the heat escapes into the sapphire substrate from the normal segment of the wire, where the heat was generated. As we were unable to find any information on α for a NbN-sapphire system in literature, the value of α used in our model (see

TABLE I
PARAMETER VALUES

d (nm)	ρ (Ωm)	α (W/m^{2}K)	c_e (J/m^{3}K)	c_p (J/m^{3}K)	T_{sub} (K)
4	2.4×10^{-6}	8×10^{5} [a]	2400 [b]	9800 [b]	2

[a] Thermal boundary conductivity at 10 K.
[b] specific heat at 10 K from Ref. [5].

Table I) was obtained from an estimate based on our hysteretic I-V measurements.

The final parameter used in our model, the thermal conductivity of NbN κ, was state and temperature dependent. By applying the Wiedemann-Franz law ($\kappa = LT/\rho$, where $L = 2.45 \times 10^{-8}$ WΩ/K^2 is the Lorenz number), we can calculate the temperature dependence of the normal state thermal conductivity κ_n with the knowledge of ρ. The superconducting state thermal conductivity κ_s was calculated such that $\kappa_s/\kappa_n = T/T_c$ similar to the treatment used in [9]. We also ignored the phonon contribution to κ which should be very small for a thin film and at the low temperatures under consideration. The phonon mean free path is very short in a thin film and the phonon contribution to the thermal conductivity is negligible compared to the electronic contribution [15].

B. Electrical Model

Electrically, the SNSPD was modeled as an inductor in series with a resistor as shown in Fig. 1(b). The inductor L_k represented the kinetic inductance of the superconducting nanowire as explained in [5]. The resistance R_n in series with the inductor was the total resistance formed from a contiguous number of segments that switch into the normal state.

Experimentally, we bias our devices using a bias tee and a low-noise current source. The DC port of the bias tee was modeled as a constant current source and a capacitor C_{bt} was included to represent the AC port. The impedance Z_o of the transmission line connecting the probe to RF amplifiers was modeled as a 50 Ω load. We solved for the current I through the nanowire using the following equation.

$$C_{bt}\left(\frac{d^2L_kI}{dt^2} + \frac{d(IR_n)}{dt} + Z_o\frac{dI}{dt}\right) = I_{bias} - I \qquad (5)$$

Note in (5) that R_n is coupled to the thermal model and is not a constant value. The thermal model determines the length of the normal region which is proportional to R_n. We used the Crank-Nicholson finite difference method in our simulations to solve (1) and (5). A summary of the parameter values used in our simulations is shown in Table I.

III. RESULTS

Using the simple model explained in Section II, we were able to simulate the growth of the normal region along the wire, the change in current through the wire and the temperature increase along the wire after the formation of a resistive barrier.

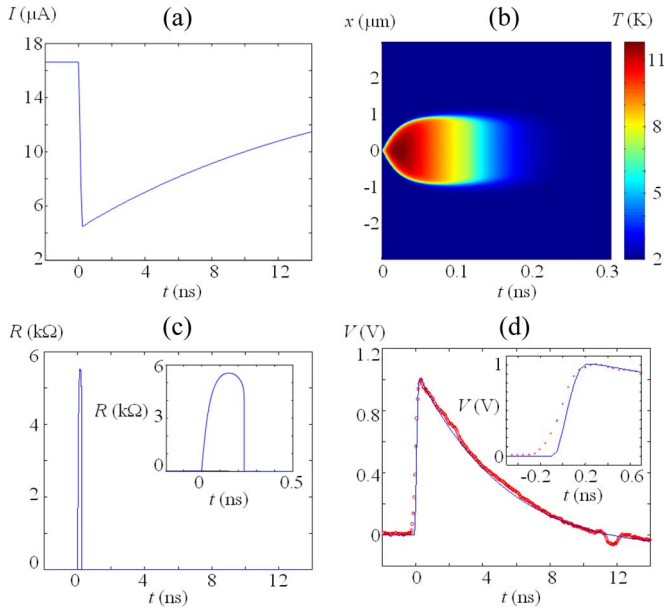

Fig. 2. (a) Plot of calculated current through an SNSPD with $L_k = 807.7$ nH vs time. The photon-induced resistive barrier forms at $t = 0$. (b) Map of calculated temperature (shown using colors) at different positions along the wire and in time. Calculations show that the wire temperature increases to a maximum value of ~12 K. (c) Plot of calculated total normal state resistance vs time. Inset shows in greater detail the gradual increase of the resistance at $t = 0$ and a sharper decrease back into the superconducting state at $t = 230$ ps. (d) Plot of calculated voltage pulse (solid line) in comparison to an experimentally measured time-averaged pulse (red circles). The undershoot in voltage below 0 V was due to the high-pass cutoff of the RF amplifiers while the dip at ~12 ns was due to reflections along the transmission line. Inset shows the rising edge of the voltage pulse. The rise time of the numerical result was shorter than that of the measured pulse.

The calculated current through the wire is shown in Fig. 2(a). A plot of the calculated temperature along the wire as time progresses is shown in Fig. 2(b). The calculated resistance along the wire is as shown in Fig. 2(c). The voltage pulse at the output due to the dip in current through the device can be calculated by multiplying the calculated amount of current dip with the transmission line impedance, scaling it by the total voltage amplification, and high-pass filtering the signal to get the calculated signal after passing through the various RF components used in experiments. In Fig. 2(d), this calculated response with no free parameters is compared to a typical voltage pulse (time averaged) obtained for an SNSPD with a measured kinetic inductance of 807.7 nH. A scanning-electron micrograph image of such a device is shown in Fig. 3(b). We chose to use a device with a large kinetic inductance so that the rise times of the pulses are long enough to be observable on a 6-GHz real-time oscilloscope. The agreement between calculation and experimental data was good.

The calculations show that the temperature of the wire increases due to Joule heating to a maximum value of about 12 K. The calculations also tell us that the resistance of the device R_d builds up to a maximum value of about 5.5 kΩ and that the current through the wire dips not all the way to zero but only to ~20% of its original value.

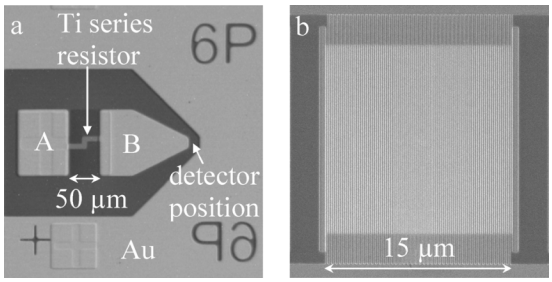

Fig. 3. (a) Optical micrograph of the Au contact pads used to make electrical connection to the SNSPD. The titanium resistor bridges pads A and B. This configuration permitted us to bias the SNSPD through the resistor by landing the probe at position A or to bypass the resistor by landing the probe at position B. The outer Au pad was at signal ground. (b) Scanning-electron micrograph (SEM) of a 15-by-15-μm meander SNSPD with a 50% fill factor, wire width of 100 nm and total wire length of $\sim$1 mm.

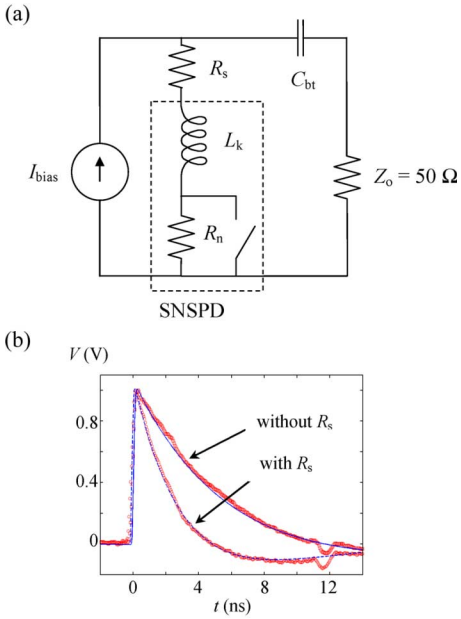

Fig. 4. (a) Schematic of modified electrical model after adding a resistor R_s in series with the SNSPD. The added series resistance will reduce the reset time of the detectors by lowering the time constant. (b) Comparison of voltage pulses measured with and without $R_s = 192\ \Omega$, showing a shortening of the reset time when the SNSPD was biased through R_s. The actual speed-up was about a factor of five although this speedup is not clear from the plots here due to the high-pass cutoff at 20 MHz, which makes long pulses look shorter. The dashed and solid lines are the simulation results for SNSPDs biased with and without R_s respectively. We used the same bias currents when measuring both voltage pulses resulting in the same pulse height of $\sim$1 V after $\sim$48 dB signal amplification.

IV. Increasing the Speed of SNSPDs

The time constant for the resetting of SNSPDs [5] is equal to the ratio of its kinetic inductance L_k to the impedance connected across it, i.e. the L/R time constant. One can increase the device speed by reducing this L/R time constant. Reducing L_k would require reducing the total length of the nanowire. This reduction in length would lead to either a smaller active area or a lower fill-factor meander, both of which are detrimental to the detection efficiency of the device. We chose instead to increase the resistance "seen" by the device by adding a resistor in series with the device.

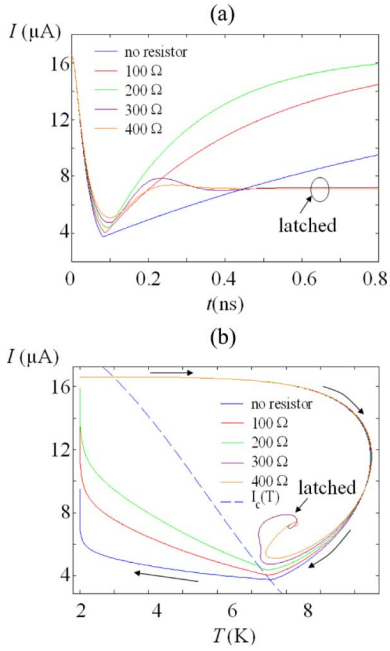

Fig. 5. (a) Plot of current through the nanowire vs time for a device with $L_k = 60$ nH. Legend shows value of R_s in ohms. Device latches when $R_s > 200\ \Omega$ and the current does not "reset" to its original value. (b) Plot of hotspot $I - T$ trajectories for different values of R_s. The dashed line is the I_c vs T plot following equation (2). Arrows show the direction of movement of trajectory in $I - T$ space as time progresses. Devices that latch do not cross into the superconducting side of the I_c vs T plot.

We fabricated an on-chip Ti resistor in series with the detector as shown in the optical micrograph of Fig. (3a) and the schematic of Fig. 4(a). Using our model, we calculated the effect that this modification had on device performance. As shown in Fig. 4(b), our model accurately predicts the speed up in device performance due to the series resistance. The series resistance value was 192 Ω, and the reduction in the L/R time constant by a factor of five resulted in a device speed-up by the same factor. Note in these calculations that the full electrothermal model was used only to determine the rising edge of the voltage pulse (i.e. when the resistor in the electrical model depended on the size of the growing or decaying hotspot). Once the wire switched back into the superconducting state, the electrical model was decoupled from the thermal model. Hence only the electrical model is relevant when calculating the resetting of the SNSPD.

When we tried to speed up the devices further by using progressively larger resistors, we observed a device latching behavior. Our model calculations for increasing values of the series resistance show a similar trend. In our calculations on device latching, we used $L_k = 60$ nH instead of 807.7 nH. Fig. 5(a) shows the current through the nanowire at different times for several values of R_s. We see that for values of $R_s > 200\ \Omega$, latching occurs and the device does not reset, i.e. the current does not increase back to its original value but settles to a stable value.

Fig. 5(b) shows numerical results of the trajectories in current and hotspot-temperature space for devices biased through different values of R_s. Notice that latching does not occur if the trajectory crosses into the superconducting domain of the

I_c vs T plot. On the other hand, latching occurs when there is insufficient decrease in the current and heating persists in the hotspot. Within the nanosecond time frame, the trajectories in this case settle into a stable state in the resistive domain of the I_c vs T plot. This state occurs when the heat generated due to Joule heating is equal to the heat dissipated into the substrate and along the wire. Thus a self-heating hotspot is temporarily sustained. Over a much longer time scale (set by the RC time constant) the current through the wire will rise back to its original value because the bias current has no other path to ground other than through the nanowire. A runaway effect would then occur as the increasing current drives the entire nanowire normal.

V. Conclusion

We found that the electro-thermal model was able to predict that a voltage pulse would result after the onset of a resistive barrier across the nanowire biased close to I_c. We show that Joule heating is responsible for the growth of a large normal region along the wire resulting in a rise time in the voltage output in the order of $\sim$100 ps. Once the current has dropped below a certain threshold value, the wire switches back into the superconducting state and the current through the wire will begin to recover to its initial value.

We then modified the electrical model by adding a resistor in series with the SNSPD and simulated an increase in the detector speed. We presented preliminary experimental results of this device speed-up. In this experiment, we biased the device through a Ti resistor that was fabricated on-chip and in series with the SNSPD. Experimental results show that a speed-up by a factor of five could be achieved for a large 15 by 15 μm active-area device biased through a 192 Ω resistor.

Finally, we observed, both experimentally and through simulations, an upper limit to speeding up the devices using the series-resistor method. We saw a new SNSPD latching behavior when the series resistor value was too high. Initial tests indicate that the SNSPD enters into a regime where a thermally stable, self-heating hotspot forms.

Acknowledgment

The authors thank R. J. Ram for use of his equipment, H. I. Smith for use of his equipment and facilities, M. K. Mondol for technical assistance with electron-beam lithography, J. M. Daley for technical assistance and helpful discussions regarding fabrication. The authors would also like to thank T. P. Orlando for helpful discussions, and G. N. Gol'tsman and B. Voronov for providing us with NbN films.

References

[1] K. M. Rosfjord, J. K. W. Yang, E. A. Dauler, A. J. Kerman, V. Anant, B. M. Voronov, G. N. Gol'tsman, and K. K. Berggren, "Nanowire single-photon detector with an integrated optical cavity and anti-reflection coating," *Optics Express*, vol. 14, pp. 527–534, 2006.

[2] J. Zhang, W. Slysz, A. Verevkin, O. Okunev, G. Chulkova, A. Korneev, A. Lipatov, G. N. Gol'tsman, and R. Sobolewski, "Response time characterization of NbN superconducting single-photon detectors," *IEEE Transactions on Applied Superconductivity*, vol. 13, pp. 180–183, 2003.

[3] J. Kitaygorsky, J. Zhang, A. Verevkin, A. Sergeev, A. Korneev, V. Matvienko, P. Kouminov, K. Smirnov, B. Voronov, G. Gol'tsman, and R. Sobolewski, "Origin of dark counts in nanostructured NbN single-photon detectors," *IEEE Transactions on Applied Superconductivity*, vol. 15, pp. 545–548, 2005.

[4] G. N. Gol'tsman, O. Okunev, G. Chulkova, A. Lipatov, A. Semenov, K. Smirnov, B. Voronov, A. Dzardanov, C. Williams, and R. Sobolewski, "Picosecond superconducting single-photon optical detector," *Applied Physics Letters*, vol. 79, pp. 705–707, 2001.

[5] A. J. Kerman, E. A. Dauler, W. E. Keicher, J. K. W. Yang, K. K. Berggren, G. Gol'tsman, and B. Voronov, "Kinetic-inductance-limited reset time of superconducting nanowire photon counters," *Applied Physics Letters*, vol. 88, p. 111116, 2006.

[6] J. K. W. Yang, E. Dauler, A. Ferri, A. Pearlman, A. Verevkin, G. Gol'tsman, B. Voronov, R. Sobolewski, W. E. Keicher, and K. K. Berggren, "Fabrication development for nanowire GHz-counting-rate, single photon detectors," *IEEE Transactions on Applied Superconductivity*, vol. 15, pp. 626–630, 2005.

[7] A. Rothwarf and B. N. Taylor, "Measurement of recombination lifetimes in superconductors," *Physical Review Letters*, vol. 19, p. 27, 1967.

[8] K. S. Il'in, M. Lindgren, M. Currie, A. D. Semenov, G. N. Gol'tsman, R. Sobolewski, S. I. Cherednichenko, and E. M. Gershenzon, "Picosecond hot-electron energy relaxation in NbN superconducting photodetectors," *Applied Physics Letters*, vol. 76, pp. 2752–2754, 2000.

[9] M. Tinkham, J. U. Free, C. N. Lau, and N. Markovic, "Hysteretic I-V curves of superconducting nanowires," *Physical Review B*, vol. 68, p. 134515, 2003.

[10] W. J. Skocpol, M. R. Beasley, and M. Tinkham, "Self-heating hotspots in superconducting thin-film microbridges," *Journal of Applied Physics*, vol. 45, pp. 4054–4066, 1974.

[11] A. D. Semenov, G. N. Gol'tsman, and A. A. Korneev, "Quantum detection by current carrying superconducting film," *Physica C*, vol. 351, pp. 349–356, 2001.

[12] M. Tinkham, *Introduction to Superconductivity*, 2nd ed. New York: McGraw Hill, 1996.

[13] E. T. Swartz and R. O. Pohl, "Thermal-boundary resistance," *Reviews of Modern Physics*, vol. 61, pp. 605–668, 1989.

[14] S. Sahling, J. Engert, A. Gladun, and R. Knoner, "The thermal-boundary resistance between sapphire and aluminum mono-crystals at low-temperature," *Journal of Low Temperature Physics*, vol. 45, pp. 457–469, 1981.

[15] A. W. Bjerkaas, D. M. Ginsberg, and B. J. Mrstik, "Electronic thermal conductivity of superconducting thin films of indium-manganese alloys," *Physical Review B*, vol. 5, p. 854, 1972.